Turk. J. Math. Comput. Sci.
16(1)(2024) 28–34

DOI : 10.47000/tjmcs.1416248

Analysis on Aperture Size for Electromagnetic Scattering by Circular Strips with Impedance Boundary Conditions

Kamil Karaçuha[1,*], Vasil Tabatadze[2]

[1]*Department of Electrical Engineering, Faculty of Electrical and Electronics, İstanbul Technical University, 34467, İstanbul, Türkiye.*
[2]*Informatics Institute, İstanbul Technical University, 34467, İstanbul, Türkiye.*

Received: 08-01-2024 • Accepted: 30-01-2024

Abstract. This study investigates how altering the aperture size and impedance characteristics of a circular strip, when excited by a cylindrical wave, influences electromagnetic scattering. The focus is on understanding the impact of shifting the position of an H-polarized line source and adjusting parameters such as strip aperture, wave number, and impedance values on the overall behavior of the electromagnetic field. Our findings reveal that changes in the strip's aperture dimensions or wave number, even when regarding the latter's relation to the source, lead to significant alterations in the surrounding electromagnetic field. This scrutiny unveils a detailed interplay between these factors within this electromagnetic scenario. By examining these intricacies, our study sheds light on the substantial impact of subtle modifications in the strip's dimensions, combined with adjustments in wave and source characteristics, on the electromagnetic field. This understanding holds promise for advancements in diverse engineering applications.

2020 AMS Classification: 34L25, 78A25, 78A45

Keywords: Analytical-numerical methods, circular strip, diffraction, impedance boundary conditions, line source, scattering.

1. Introduction

Electromagnetic scattering by conical objects has captivated researchers for decades, offering pivotal insights for electromagnetic theory, antenna theory, and remote sensing [10, 15, 19]. Furthermore, the study of electromagnetic scattering and propagation in 2D problems plays a significant role in engineering design. These problems may yield analytical solutions or provide valuable physical insights into real-life scenarios [4–6, 12]. In the past century, there was extensive research into electromagnetic or acoustic scattering by discontinuities, edges, and tips, often made under certain approximations or assumptions [3, 8, 17, 18]. Understanding diffraction from finite objects in 2D or 3D canonical problems is crucial for comprehending various engineering challenges, including aperture-type antennas, remote sensing, wave propagation in different mediums, and material characterization [1, 7, 13, 16]. Specifically, there exists an extensive body of literature on diffraction by 2D problems, approached through different methods. The proposed approach involves an integral equation based on a method where the current induced on the scatterer is represented by a carefully chosen complete set of orthogonal polynomials.

*Corresponding Author
Email addresses: karacuha17@itu.edu.tr (K. Karaçuha), vasilitabatadze@gmail.com (V. Tabatadze)

In free space, the total field around a scatterer results from the vector sum of incident and scattered field components [2,14]. In direct scattering problems, the incident field components are known beforehand, motivating the search for scattered field components. Given that electromagnetic waves for sinusoidal excitation adhere to the Helmholtz equation in a defined space with specific boundary conditions, obtaining scattered field components involves mathematically representing the field component and satisfying boundary, edge, and radiation conditions. This is achieved by representing the scattered field components through the convolution of the induced unknown current density with the corresponding Green's function [1, 12]. The unknown current density is determined by applying boundary conditions to formulate the boundary value problem. Solving this problem typically involves representing the current density using basis functions in the Method of Moments [15]. In this case, the current densities are expressed in terms of a complete set of orthogonal polynomials with unknown coefficients. Determining these coefficients involves utilizing orthogonal properties. Additionally, the proposed approach enables enforcing edge conditions by expressing current densities with suitable weighting functions, selected based on the problem's geometry and edge conditions.

The methodology proposed for solving the circular arc problem involves analytical-numerical methods. These methods provide closed-form expressions or solutions, offering insights into scattering behavior and aiding in understanding the underlying physical phenomena. They are computationally efficient, enabling rapid analysis and aiding in engineering design. Moreover, they serve as benchmarks for validating complex simulations or experimental measurements. Impedance boundary conditions are pivotal in describing electromagnetic field behavior at a scatterer's boundary. They establish the correlation between electric and magnetic fields, allowing accurate modeling of wave interactions with different scatterers, such as conducting lossy surfaces. Analyzing scattering by circular strips with impedance boundaries helps comprehend how impedance values affect resonator properties and scattering patterns, assisting in designing and optimizing electromagnetic systems. Two-dimensional problems are crucial for validating methodologies before tackling more intricate geometries. This study deviates from previous works by considering a circular strip geometry excited by cylindrical waves with varying impedance values on inner and outer surfaces. It explores resonance phenomena not observed previously and investigates location dependencies, noting higher Q-factors for specific impedance values compared to perfect conducting surfaces.

This study follows the path set by [13, 16] concerning geometry and theory. However, it takes a different direction by exploring the impact of aperture size under various boundary conditions. The investigation aims to highlight the significance of scatterer surface impedance and aperture size in shaping radiation patterns, crucial for achieving directive radiation patterns or ensuring wideband stable radiation characteristics from an engineering perspective.

2. Formulation of the Problem

In this section, the theoretical background is provided briefly since the mathematical foundations were analyzed previously extensively in [13, 16]. However, it would be substantial to give the main goal and the advantages of the proposed approach. It is worth mentioning that, the actual goal is very straightforward. First, the incident and scattered fields need to be defined *mathematically*. Then, the boundary conditions are enforced on the surface and the boundary value problem is obtained. This part is the first part of the main task. Later, the question arises of how to solve the initial value problem. There are several approaches including semi-analytical, numerical, etc [7, 13, 16]. The proposed approach considering the current densities as the infinite summation of the orthogonal polynomials on the normalized scatterer surface is under semi-analytical methods.

After giving procedure, it is time to present the total field as given in (2.1):

$$H_z = H_z^0 + H_z^S \,. \tag{2.1}$$

Here, H_z^0 stands for the incident magnetic field whereas H_z^S corresponds to the scattered field. since the excitation is from a line source, the incident cylindrical wave mathematically can be represented by (2.2):

$$H_z^0 = -ZH_0^{(1)}\left(k\left|\rho - \rho_0\right|\right). \tag{2.2}$$

Please note that $Z = \frac{k^2 A_0}{4\omega\epsilon_0}$ is a constant coefficient, where k is the wavenumber, ω is the angular frequency, ϵ_0 is the permittivity of free space, and $H_0^{(1)}$ corresponds to the Hankel functions of the first kind and zeroth order. The scattered field arises from induced currents on the scatterer surface, excited by the impressed sources. The corresponding field component can be expressed as the convolution of the current densities with the corresponding Green's function of the medium, as provided in Equation (2.3):

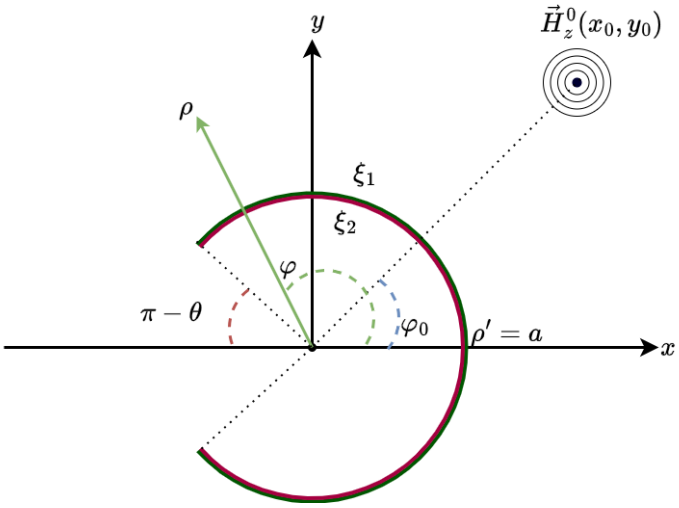

FIGURE 1. Caption for the figure

$$H_z^S = \int_{-\theta}^{\theta} \left\{ \mu^m(\varphi) + \mu^e(\varphi) \frac{\partial}{\partial (k\rho')} \right\} H_0^{(1)} \left(k \left| \rho - \rho' \right| \right) d\varphi, \rho' = a. \tag{2.3}$$

Here, μ^m and μ^e are the magnetic and electric current densities representing the scatterer.

The induced current densities are represented by the summation of the Gegenbauer polynomials C_n with unknown constant coefficients, as given in Equation (2.4). It's important to note that the strip arc is normalized within the interval $[-1, 1]$, and at the edges, the edge conditions for electric and magnetic current densities are fulfilled by the weighting functions $(1 - \eta^2)^\nu$ [9, 11, 16]. This weighting function serves not only to satisfy the edge condition but also exploits orthogonality to determine unknown coefficients, facilitating faster convergence and expediting computations [2, 13, 16].

$$\begin{aligned} \mu^e(\eta) &= \left(1 - \eta^2\right)^{\nu_1} \sum_{n=0}^{\infty} x_n C_n^{\nu_1 + \frac{1}{2}}(\eta), \\ \mu^m(\eta) &= \left(1 - \eta^2\right)^{\nu_2} \sum_{n=0}^{\infty} y_n C_n^{\nu_2 + \frac{1}{2}}(\eta), \end{aligned} \tag{2.4}$$

where $\nu_1 = -\frac{1}{2}$ and $\nu_2 = \frac{1}{2}$ to satisfy the edge condition, respectively [9].

Noticed that, the geometry is periodic in φ direction. Therefore, the scattered field can be represented by the Fourier series employing this periodicity. Further, the addition theorem for Hankel's function is used to split the argument of the Hankel function in (2.3) as provided in (2.5) [9, 11, 16].

Gegenbauer polynomials are chosen because the polynomials are defined between -1 to 1, leading to the normalization of our strip width from $[-a, a]$ to $[-1, 1]$. The second reason is that the weighting function for orthogonal is also suitable for the behavior of the current densities at the edges (edge conditions) [9, 11, 16].

$$H_z^S = \frac{4\mathrm{j}}{\varepsilon} \sum_{m=-\infty}^{\infty} \widehat{\mu}_m^m \begin{cases} J_m(k\rho) H_m^{(1)}(\varepsilon) e^{jm\varphi'} \rho < a \\ J_m(\varepsilon) H_m^{(1)}(k\rho) e^{jm\varphi'} \rho > a \end{cases} + \frac{4i}{\varepsilon} \sum_{m=-\infty}^{\infty} \widehat{\mu}_m^e \begin{cases} J_m(k\rho) H_m^{(1)'}(\varepsilon) e^{jm\varphi'} \rho < a \\ J'_m(\varepsilon) H_m^{(1)}(k\rho) e^{jm\varphi'} \rho > a \end{cases}, \tag{2.5}$$

where $\varepsilon = ka$ and

$$\widehat{\mu}_m^e = \frac{\theta}{\Gamma\left(\nu_1+\frac{1}{2}\right)}\sum_{n=0}^{\infty} j^n x_n \boldsymbol{\beta}_n^{\nu_1+\frac{1}{2}} \frac{J_{\nu_1+n+\frac{1}{2}}(-m\theta)}{(-2m\boldsymbol{\theta})^{(\nu_1+\frac{1}{2})}},$$
$$\widehat{\mu}_m^m = \frac{\theta}{\Gamma\left(\nu_2+\frac{1}{2}\right)}\sum_{n=0}^{\infty} j^n y_n \boldsymbol{\beta}_n^{\nu_2+\frac{1}{2}} \frac{J_{\nu_2+n+\frac{1}{2}}(-m\theta)}{(-2m\boldsymbol{\theta})^{(\nu_2+\frac{1}{2})}}.$$

Here $\Gamma\left(\nu+\frac{1}{2}\right)$ is the Gamma function and $\beta_n^{\nu_i+\frac{1}{2}} = \frac{\Gamma(2\nu_i+1+n)}{\Gamma(n+1)}$, and $\widehat{\mu}_m = \frac{\theta}{2\pi}\int_{-1}^{1}\mu(\eta)e^{-jm\theta\eta}d\eta$.

After expressing the field components (incident and scattered ones), it is time to force the boundary conditions from inner and outer surfaces as below:

$$\frac{\partial}{\partial k\rho}H_z \pm jk\xi_{1,2}H_z = 0, \rho = \pm a \tag{2.6}$$

(2.6) is called in general impedance boundary condition (IBC) or Leontovich boundary condition [9, 11, 16]. This is a generalized boundary condition depending on the value of $\xi_{1,2}$, the boundary condition can be approximated as well-known Dirichlet and Neumann boundary conditions for the limit cases. For validation, these limits need to be checked in numerical analysis.

The final version of the system of linear algebraic equation (SLAE) for the outer surface in case of $\rho_0 < a$ as (2.7):

$$2\pi\frac{\theta}{\Gamma\left(\nu_2+\frac{1}{2}\right)}\sum_{p=0}^{\infty}\mathrm{j}^p x_p\beta_p^{\nu_2+\frac{1}{2}}\tilde{Q}_{kp}^{11} + 2\pi\frac{\theta}{\Gamma\left(\nu_1+\frac{1}{2}\right)}\sum_{p=0}^{\infty}\mathrm{j}^p y_p\beta_p^{\nu_2+\frac{1}{2}}\tilde{Q}_{kp}^{12} = \tilde{A}_k^1. \tag{2.7}$$

Here,

$$\tilde{Q}_{kp}^{11} = \sum_{m=-\infty}^{\infty} J_m(\varepsilon)\tilde{H}_m^{(1)}\left(\frac{2}{m\theta}\right)^{\nu_1+\frac{1}{2}}\Gamma\left(\nu_1+\frac{1}{2}\right)J_{k+\nu_1+\frac{1}{2}}(m\theta)\frac{J_{\nu_2+p+\frac{1}{2}}(-m\theta)}{(-2m\theta)^{(\nu_2+\frac{1}{2})}},$$
$$\tilde{Q}_{kp}^{12} = \sum_{m=-\infty}^{\infty} J'_m(\varepsilon)\tilde{H}_m^{(1)}\left(\frac{2}{m\theta}\right)^{\nu_1+\frac{1}{2}}\Gamma\left(\nu_1+\frac{1}{2}\right)J_{k+\nu_1+\frac{1}{2}}(m\theta)\frac{J_{\nu_1+p+\frac{1}{2}}(-m\theta)}{(-2m\theta)^{(\nu_1+\frac{1}{2})}},$$
$$\tilde{A}_k^1 = \mathrm{Z}\sum_{m=-\infty}^{\infty} J_m(k\rho_0)\tilde{H}_m^{(1)}\left(\left(\frac{2}{m\theta}\right)^{\nu_1+\frac{1}{2}}\Gamma\left(\nu_1+\frac{1}{2}\right)J_{k+\nu_1+\frac{1}{2}}(m\theta)\right)e^{-\mathrm{j}m\varphi_0}.$$

The final version of the system of linear algebraic equation (SLAE) for the inner surface in case of $\rho_0 < a$ as (2.7)

$$2\pi\frac{\theta}{\Gamma\left(\nu_2+\frac{1}{2}\right)}\sum_{p=0}^{\infty}\mathrm{j}^p y_p\beta_p^{\nu_2+\frac{1}{2}}\tilde{Q}_{kp}^{21} + 2\pi\frac{\theta}{\Gamma\left(\nu_1+\frac{1}{2}\right)}\sum_{p=0}^{\infty}j^p x_p\beta_p^{\nu_1+\frac{1}{2}}\tilde{Q}_{kp}^{22} = \tilde{A}_k^2.$$

Here,

$$\tilde{Q}_{kp}^{21} = \sum_{m=-\infty}^{\infty} H_m^{(1)}(\varepsilon)\tilde{J}_{m1}\left(\frac{2}{m\theta}\right)^{\nu_1+\frac{1}{2}}\Gamma\left(\nu_1+\frac{1}{2}\right)J_{k+\nu_1+\frac{1}{2}}(m\theta)\frac{J_{\nu_2+p+\frac{1}{2}}(-m\theta)}{(-2m\theta)^{(\nu_2+\frac{1}{2})}},$$
$$\tilde{Q}_{kp}^{22} = \sum_{m=-\infty}^{\infty} H_m^{(1)'}(\varepsilon)\tilde{J}_{m1}\left(\frac{2}{m\theta}\right)^{\nu_1+\frac{1}{2}}\Gamma\left(\nu_1+\frac{1}{2}\right)J_{k+\nu_1+\frac{1}{2}}(m\theta)\frac{J_{\nu_1+p+\frac{1}{2}}(-m\theta)}{(-2m\theta)^{(\nu_1+\frac{1}{2})}},$$
$$\tilde{A}_k^2 = \mathrm{Z}\sum_{m=-\infty}^{\infty} J_m(k\rho_0)\tilde{H}_{m1}\left(\left(\frac{2}{m\boldsymbol{\theta}}\right)^{\nu_1+\frac{1}{2}}\Gamma\left(\nu_1+\frac{1}{2}\right)J_{k+\nu_1+\frac{1}{2}}(m\boldsymbol{\theta})\right)e^{-\mathrm{j}m\varphi_0}.$$

Here, $\tilde{J}_m = J'_m(\varepsilon) + jk\xi_1 J_m(\varepsilon)$,$\tilde{H}_m^{(1)} = H_m^{(1)'}(\varepsilon) + \mathrm{j}k\xi_1 H_m^{(1)}(\varepsilon)$ and $\tilde{J}_{m1} = J'_m(\varepsilon) - \mathrm{j}k\xi_2 J_m(\varepsilon)$.

For the source located outside the circular strip ($\rho_0 > a$), the same procedure can be followed and results can be obtained as provided in [13, 16].

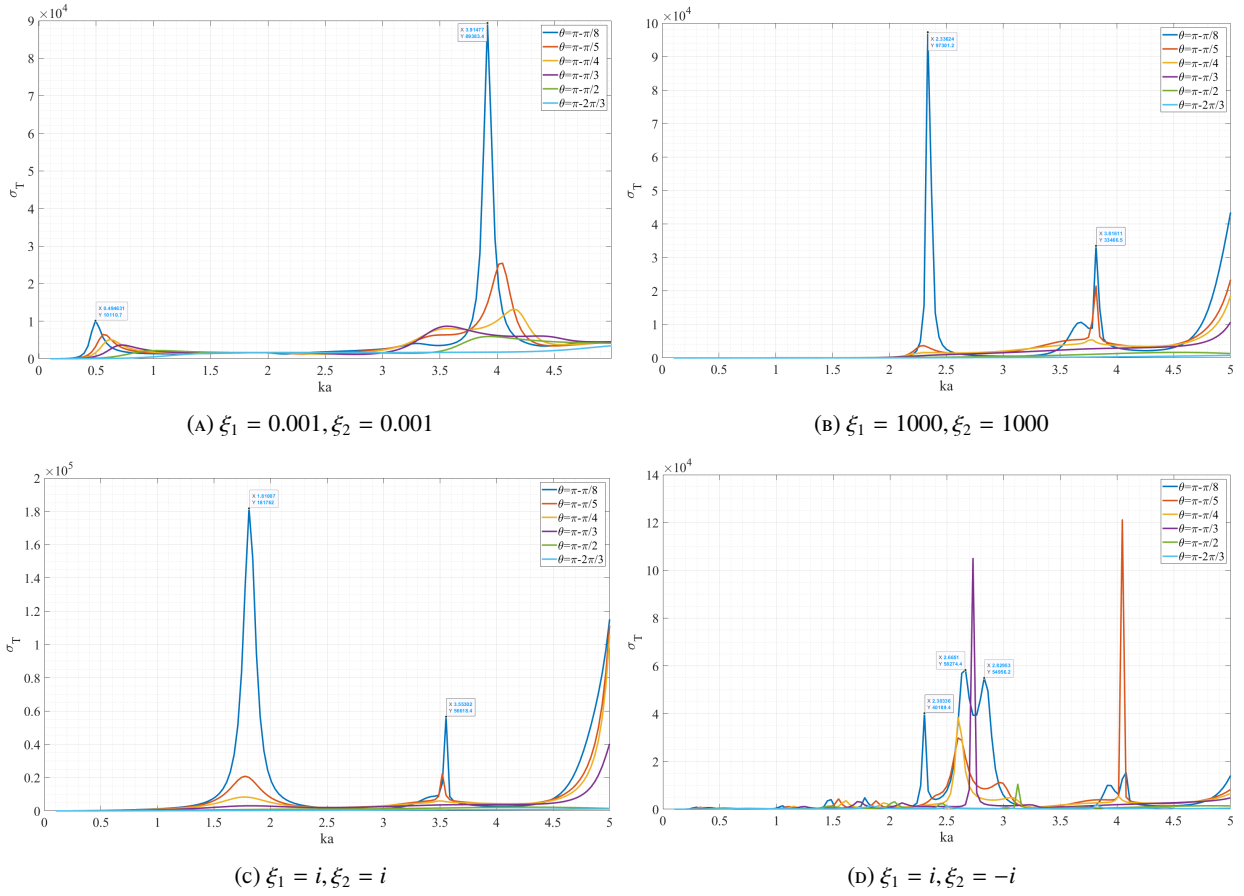

(A) $\xi_1 = 0.001, \xi_2 = 0.001$

(B) $\xi_1 = 1000, \xi_2 = 1000$

(C) $\xi_1 = i, \xi_2 = i$

(D) $\xi_1 = i, \xi_2 = -i$

FIGURE 2. TRCS for different parameters ($a = 1$, $x_0 = y_0 = 0.01$)

3. NUMERICAL RESULTS

In this section, numerical results for TRCS are presented, encompassing various scenarios. Different cases involving diverse aperture sizes, impedance values, and source locations are investigated to observe resonances and their characteristics. Notably, when the aperture size is considerably smaller than the incident wavelength, resonance values tend to approach the zeros of Bessel functions and their derivatives for Dirichlet and Neumann boundary conditions, respectively, aligning with expectations. In the case of H-polarization, perfect magnetic conducting (PMC) and perfect electric conducting (PEC) surfaces serve as the limit cases for the Leontovich boundary conditions [13, 16].

We explore TRCS with the line source positioned at the center, as depicted in Figure 2. Figure 2a represents the PEC surface, while Figure 2b corresponds to the PMC surface, approximating the Dirichlet boundary conditions due to resonances observed at Bessel function zeros for very small apertures relative to the incident wavelength ($\theta = \pi - \frac{\pi}{8}$). When impedance values become imaginary (inductive and capacitive surfaces), notable changes in resonance characteristics occur, as observed in Figure 2c and Figure 2d. Particularly, when the surface exhibits inductive and capacitive behavior simultaneously, a double resonance effect is evident, leading to increased resonance bandwidth, as depicted in Figure 2b.

Later, we investigate the same boundary conditions for the source located far-field to verify our results with plane wave excitations as given in Figure 3 [13, 16]. As expected, values of TRCS are decreased since the line source has $1/\sqrt{\rho}$ behavior when it is at the far zone. Again, the same boundary conditions and surface impedance values are employed. As it is noticed when the resonator has the surface impedance of complex conjugate pair, there exist numerous resonances as given in Figure 3d [13, 16].

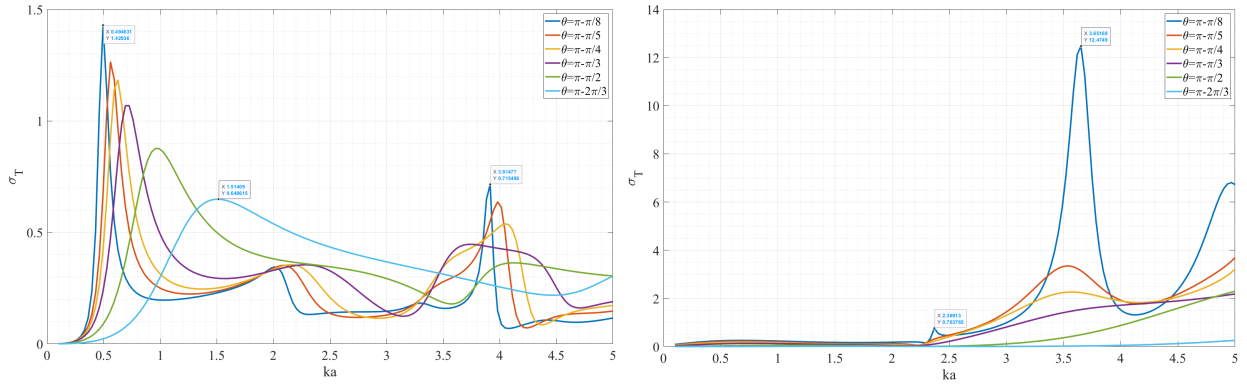

(A) $\xi_1 = 0.001, \xi_2 = 0.001$ (B) $\xi_1 = 1000, \xi_2 = 1000$

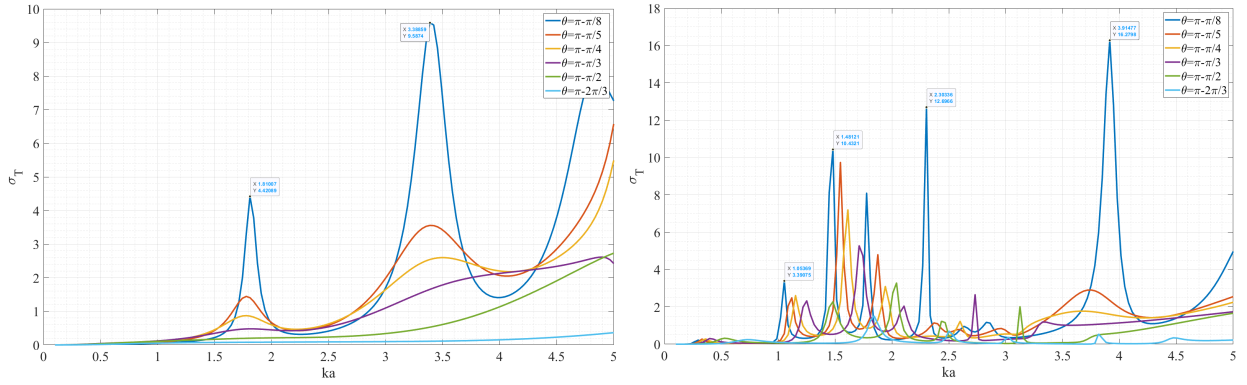

(C) $\xi_1 = i, \xi_2 = i$ (D) $\xi_1 = i, \xi_2 = -i$

FIGURE 3. TRCS for different parameters ($a = 1$, $x_0 = -1000, y_0 = 0$)

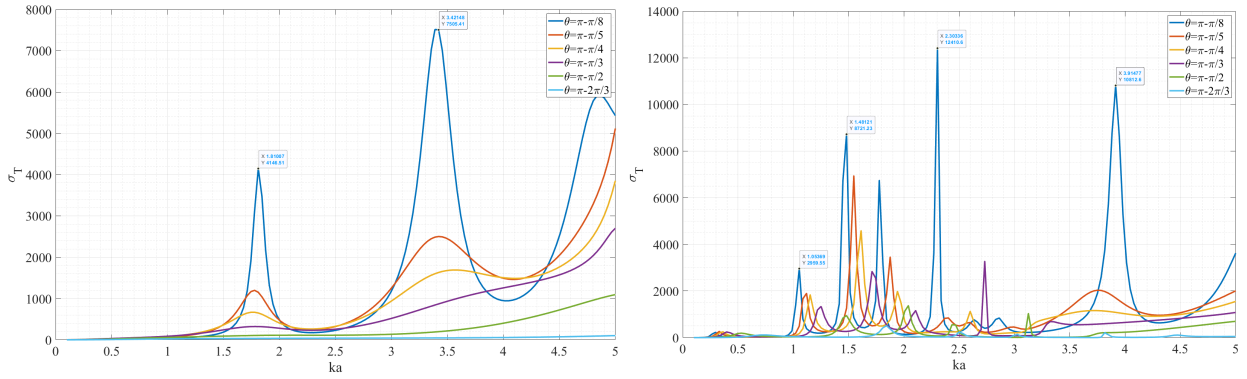

(A) $\xi_1 = i, \xi_2 = i$ (B) $\xi_1 = i, \xi_2 = -i$

FIGURE 4. TRCS for different parameters ($a = 1$, $x_0 = -2, y_0 = 0$)

Lastly, the line source is located close to the aperture of the resonator structure Figure 4. Similar characteristics are obtained when it is compared to Figure 3.

4. Conclusion

This study reveals the impact of aperture size on the diffraction characteristics of a circular strip with varying impedance values. Examining different source locations sheds light on how both aperture size and impedance values influence the overall field distribution. Notably, both parameters—impedance value and aperture size—exhibit significant effects on the total field distribution. Moreover, alterations in these parameters lead to distinct variations in resonance characteristics. Particularly, the aperture size demonstrates a crucial qualitative influence on the directivity of the scattered field, aligning with expectations. The method's strength lies in its incorporation of edge conditions into the system of linear algebraic equations (SLAE), resulting in expedited convergence and a smaller matrix dimension for inversion. This advantage facilitates more efficient and precise analysis of the diffraction problem, showcasing the method's efficacy in handling complex scenarios involving variable impedance values and aperture sizes.

Conflicts of Interest

The authors declare that there are no conflicts of interest regarding the publication of this article.

Authors Contribution Statement

All authors have read and agreed to the published version of the manuscript.

References

[1] Alparslan, A., *Spectral analysis of line sources with complex longitudinal wavenumbers in planarly layered media*, IEEE Transactions on Antennas and Propagation, **69**(1)(2020), 429–442.

[2] Dikmen, F., Karaçuha, E., Tuchkin, Y.A., *Scalar wave diffraction by a perfectly soft infinitely thin circular ring*, Turkish Journal of Electrical Engineering and Computer Sciences, **9**(2)(2001), 199–220.

[3] Doğan, M., Dikmen, F., Alkumru, A., *Line source diffraction by perfectly conducting successive steps*, Wave Motion, **68**(2017), 253–271.

[4] Erden, F., Tretyakov, O., Cosan, A.A., *Inertial properties of the TE waveguide fields*, Progress In Electromagnetics Research M, **68**(2018), 11–19.

[5] Gürbüz, T.U., Aslanyürek, B., *A Semi-Analytical Method for Electromagnetic Scattering by Infinitely Long Arbitrary Shaped Multilayer Cylinders at Oblique Incidence*, IEEE Transactions on Antennas and Propagation, (2023).

[6] Hacıvelioğlu, F., Uslu, M.A., Sevgi, L., *A MATLAB-based virtual tool for the electromagnetic wave scattering from a perfectly reflecting wedge*, IEEE Antennas and Propagation Magazine, **53**(6)(2011), 234–243.

[7] Karaçuha, K., Tabatadze, V., Alperen, Ö.F., Veliev, E., *A new approach in electromagnetic plane wave diffraction by two concentric slotted cylinders with variably placed slits: E and H polarized cases*, IET Microwaves, Antennas, and Propagation, **16**(7)(2022), 437–450.

[8] Koshovy, G.I., *Mathematical models of acoustic wave scattering by impedance strip*, In 2017 XXIInd IEEE International Seminar/Workshop on Direct and Inverse Problems of Electromagnetic and Acoustic Wave Theory (2017),71–74.

[9] Meixner, J., *The behavior of electromagnetic fields at edges*, IEEE Trans. Antennas Propag., **20**(4)(1972), 442–446.

[10] Oğuzer, T., Kutluay, D., *Localized Green's function using a beam-pattern for the fast modeling of 2D electromagnetic scattering*, Journal of Electromagnetic Waves and Applications, **36**(18)(2022), 2804–2826.

[11] Prudnikov, A.P., Brychkov, I.A., Marichev, O.I., Integrals and Series: Special Functions, vol. 2. CRC Press, 1986.

[12] Richard, L., Nosich, A.I., Daniel, J.P., *Surface-impedance model analysis of a coated cylinder with application to wave propagation and conformal antennas*, In IET Tenth International Conference on Antennas and Propagation, (1997), 123–125.

[13] Tabatadze, V., Karaçuha, K., Alperen, Ö.F., Veliev, E., *H-polarized plane wave diffraction by a slotted cylinder with different surface impedances: Solution by the analytical—Numerical approach*, IET Microwaves, Antennas, and Propagation, **16**(14)(2022), 869–879.

[14] Tabatadze, V., Karaçuha, K., Zaridze, R., Veliyev, E., Karaçuha, E., *A fundamental approach: E-polarized electromagnetic wave diffraction by two dimensional arbitrary-shaped objects with impedance boundary condition*, Journal of Electrical Engineering, **73**(6)(2022), 426–431.

[15] Tabatadze, V., Karaçuha, K., Zaridze, R., *Electromagnetic scattering from 2-D conducting objects with arbitrary smooth shape: Complete mathematical formulation of the method of auxiliary sources for E-polarized case*, Progress In Electromagnetics Research M, **114**(2022), 117–125.

[16] Tabatadze, V., Alperen, Ö.F., Karaçuha, K., *Electromagnetic scattering of H-polarised cylindrical wave by a double-sided impedance circular strip*. IET Microwaves, Antennas and Propagation, (2023).

[17] Topsakal, E., Büyükaksoy, A., İdemen, M., *Scattering of electromagnetic waves by a rectangular impedance cylinder*, Wave Motion, **31**(3)(2000), 273–296.

[18] Umul, Y.Z., *General expression of the diffracted waves by a half-screen with generalized impedance boundary conditions*, Optik, **178**(2019), 892–901.

[19] Vinogradov, S.S., Smith, P.D., Vinogradova, E.D., Canonical problems in scattering and potential theory part II: Acoustic and electromagnetic diffraction by canonical structures, CRC Press, 2002.